

# Testing MSW effect in Supernova Explosion with Neutrino event rates

Kwang-Chang Lai,<sup>1</sup> C. S. Jason Leung,<sup>2</sup> and Guey-Lin Lin<sup>2</sup>

<sup>1</sup>*Center for General Education, Chang Gung University, Kwei-Shan, Taoyuan, 333, Taiwan*

<sup>2</sup>*Institute of Physics, National Chiao Tung University, Hsinchu, 300, Taiwan*

Flavor transitions in supernova neutrinos are yet to be determined. We present a method to probe whether or not the Mikheyev-Smirnov-Wolfenstein effects occur as SN neutrinos propagate outward from the SN core by investigating time evolutions of neutrino event rates for different flavors in neutrino detectors. As the MSW effect occurs, the  $\nu_e$  flux swaps with the  $\nu_x$  flux, which represents any one of  $\nu_\mu$ ,  $\nu_\tau$ ,  $\bar{\nu}_\mu$ , and  $\bar{\nu}_\tau$  flux, either fully or partially depending on the neutrino mass hierarchy. During the neutronization burst, the  $\nu_e$  emission evolves in a much different shape from the emissions of  $\bar{\nu}_e$  and  $\nu_x$  while the latter two evolve in a similar pattern. Meanwhile, the luminosity of the  $\nu_e$  emission is much larger than those of the  $\bar{\nu}_e$  and  $\nu_x$  emissions while the latter two are roughly equal. As a consequence, the time-evolution pattern of the  $\nu_e$ Ar event rates in the absence of the MSW effect will be much different from that in the occurrence of the MSW effect, in either mass hierarchy. With the simulated SN neutrino emissions, the  $\nu_e$ Ar event rates are evaluated. The cumulative event rates of  $\nu_e$ Ar are calculated with different SN simulations up to 100 ms. We show that the time evolutions of this cumulative rates can effectively determine whether MSW effects really occur for SN neutrinos or not.

PACS numbers: 95.85.Ry, 14.60.Pq, 95.55.Vj

## I. INTRODUCTION

Flavor transitions of SN neutrinos have been an attractive field of research and motivated numerous efforts (See [1] for a review) on flavor changing during the gravitational core collapse of a massive star. Originating from deep inside the SN core, neutrinos are expected to experience significant flavor transitions as they propagate outward to the terrestrial detectors. On account of MSW effects  $\nu_e$  and  $\bar{\nu}_e$  fluxes will swap with  $\nu_x$  flux fully

or partially when the neutrino vacuum oscillation frequency  $\omega = \Delta m^2/2E$  is of the order of the matter potential,  $\lambda = \sqrt{2}G_F n_e$ . Here  $\Delta m^2$  denotes one of the mass-squared differences,  $E$  the neutrino energy, and  $n_e$  the net electron density. For typical SN post-bounce matter profiles, this MSW-induced flavor conversions occur at distances of  $\sim \mathcal{O}(10^3)$  km from the SN core where  $\omega \simeq \lambda$  [2].

In the deep region of the core where the neutrino densities are large, the off-diagonal  $\nu - \nu$  potential,  $\mu \sim \sqrt{2}G_F n_\nu$ , arising from coherent  $\nu - \nu$  forward scatterings, may induce collective pair flavor oscillation  $\nu_e \bar{\nu}_e \leftrightarrow \nu_x \bar{\nu}_x$  with a frequency  $\sim \sqrt{\omega\mu}$  over the entire energy range. Based on theoretical understanding and numerical calculations, large collective flavor conversions were predicted to occur at distances of  $\sim \mathcal{O}(10^2)$  km from the SN core where  $\omega \simeq \mu$  [3–5].

Very close ( $\sim \mathcal{O}(1)$  m) to the SN surface, the  $\nu - \nu$  potential may induce even faster flavor conversions at a rate  $\sim \mu$  than the above collective oscillation at a rate  $\sim \sqrt{\omega\mu}$  [6]. This fast flavor conversion requires sufficiently different angular distributions for different neutrino flavors [7–9]. Since the flavor  $\nu_x$  decouples from matter earlier than  $\bar{\nu}_e$ , and the latter decouples earlier than  $\nu_e$ , it can be expected that the radius of  $\nu_e$  sphere,  $r_{\nu_e}$ , is larger than that of  $\bar{\nu}_e$  sphere,  $r_{\bar{\nu}_e}$ , which in turn should be larger than  $r_{\nu_x}$ . Therefore, close to the SN surface,  $r_{\nu_e}$ , the  $\nu_x$  zenith-angle distribution would be more forward-peaked than that of  $\bar{\nu}_e$ , which in turn would be more forward-peaked than the  $\nu_e$  distribution.

Flavor transitions are expected to change flavor compositions of primary SN neutrino fluxes, and consequently to leave imprints in neutrino events measured by terrestrial detectors. This motivates us to study neutrino flavor transitions with measurements of galactic SN neutrinos arriving at the Earth. Unlike the status of MSW effects, consensus on collective flavor transitions has not yet been reached so that studies of collective flavor transition effects on terrestrial SN neutrino fluxes are few. Meanwhile, the study of fast flavor conversions has just started in recent years and is still far from a thorough understanding. Therefore, we focus on MSW effects in SN neutrinos. Based on the understanding that MSW effects are sensitive to neutrino mass hierarchy (NMH), lots of studies [10–16] are devoted to probing NMH with SN neutrino events detected on the Earth. Naturally, these studies all assume the occurrence of MSW effects. In this paper, we however would like to determine whether MSW effects really occur in SN neutrinos or not.

The paper is organized as follows. In Sec. II, we briefly review the flavor transitions of SN

neutrinos as they propagate outward from deep inside a SN and traverse the Earth medium to reach the detector. We then summarize SN neutrino fluxes obtained from the simulated SN neutrino data, which will be used in our later analysis. In Sec. III, we define the event rate of  $\nu_e$ Ar interaction inside liquid argon detector. This event rate is then calculated with respect to different flavor transition scenarios. In Sec. IV, we test the occurrence of MSW effects in SN neutrinos by comparing the time-evolution patterns of  $\nu_e$ Ar event rates with and without MSW effects in the neutrino flavor transitions with statistical uncertainties taken into account. Finally, in Sec. V we summarize our results and conclude.

## II. SUPERNOVA NEUTRINO FLUENCE

### A. Primary Neutrino Flux

A SN neutrino burst lasts for  $\Delta t \approx 10$ s, during which the neutronization burst happens at  $t_{pb} \sim 10 - 15$ ms. Here,  $t_{pb}$  denotes the post-bounce time. In our calculation, the primary neutrino fluxes are extracted from SN simulations accounting for SNe with iron core. Many efforts on simulating SN explosion have been pursued by different groups (see [17, 18] for example). For our purpose to demonstrate a phenomenological approach using the expected event rates in terrestrial detectors, we take four different simulations for roughly similar progenitor masses for the SN neutrino emissions. These simulations are for progenitor masses of  $8.8 M_\odot$  by Garching group [17], of  $10 M_\odot$  by Burrow *et al.* [18], of  $11.2 M_\odot$  by Fischer *et al.* [19], and of  $13 M_\odot$  by Nakazato *et al.* [20].

The luminosity and emission curves are shown in Fig. 1, in which, from left to right, are the Garching simulation (G-model), Burrow *et al.*'s simulation (B-model), Fischer *et al.*'s simulation (F-model), and Nakazato *et al.*'s simulation (N-model). Clearly, the patterns in the N-model is quite different from those of the other models while the patterns in the G-, B-, and F-models are similar with one another. In the N-model, the neutronization burst happens at  $t_{pb} \sim 10$ ms with its full width at half maximum of the luminosity  $\Delta t_N \sim 30$  ms while, in the other models, it happens earlier with the width of  $\Delta t_N \sim 10$  ms. It is seen that the peak height is twice that of the tail in the N-models while it is about 10 times in the other models. To encompass the whole duration of the neutronization burst, we perform our analysis for a time period of  $\Delta t = 0.1$  s from the start.

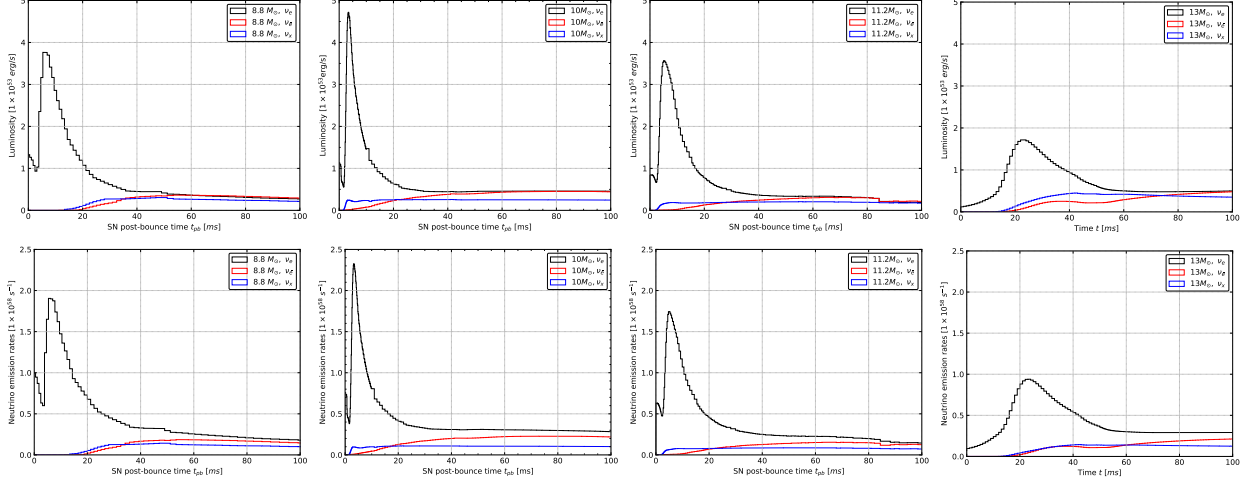


FIG. 1: Luminosities  $\mathcal{L}_\alpha$  on the upper panel and emissions  $n_\alpha$  on the lower panel in the G-, B-, F-, and N-models for progenitor masses of  $8.8 M_\odot$ ,  $10 M_\odot$ ,  $11.2 M_\odot$ , and  $13 M_\odot$  from left to right, respectively.

These SN neutrino spectra can be well fitted by the Keil parametrization for the neutrino flux [21]

$$F_\alpha^0(E, t) = \frac{\Phi_\alpha}{\langle E_\alpha \rangle} \frac{(1 + \eta_\alpha)^{(1+\eta_\alpha)}}{\Gamma(1 + \eta_\alpha)} \left( \frac{E}{\langle E_\alpha \rangle} \right)^{\eta_\alpha} \exp \left[ -(\eta_\alpha + 1) \frac{E}{\langle E_\alpha \rangle} \right], \quad (1)$$

where  $\Phi_\alpha = \mathcal{L}_\alpha / \langle E_\alpha \rangle$ ,  $\langle E_\alpha \rangle$  is the average neutrino energy, and  $\eta_\alpha$  denotes the pinching of the spectrum. For the period of interest,  $0 \leq t \leq 0.1$  s, we summarize the relevant parameters in Table I. The mean energies,  $(\langle E_{\nu_e} \rangle, \langle E_{\nu_\mu} \rangle, \langle E_{\nu_x} \rangle)$  in the G-model are the most degenerate while those in the N-model are the most diverse. While  $\langle E_{\nu_e} \rangle$ 's are  $\sim 10$  MeV in all the four models,  $\langle E_{\nu_x} \rangle$  ranges from 9.9 MeV in the G-model to 18.7 MeV in the N-model.

## B. Neutrino Flux on Earth

In this paper, we investigate whether or not the flavor contents of SN neutrinos are modified by the MSW effect as they propagate outwards from deep inside a SN and finally reaches the Earth. If MSW effects do not occur, the flavor contents at the Earth are incoherent superpositions of the mass eigenstates leaving from the SN and can be written as

$$F_\beta = P(\nu_\alpha \rightarrow \nu_\beta) F_\alpha^0, \quad (2)$$

Simulation model [M <sub>⊙</sub> ]	G			B			F			N		
Flavor	$\nu_e$	$\bar{\nu}_e$	$\nu_x$	$\nu_e$	$\bar{\nu}_e$	$\nu_x$	$\nu_e$	$\bar{\nu}_e$	$\nu_x$	$\nu_e$	$\bar{\nu}_e$	$\nu_x$
$\langle E \rangle$ [MeV]	9.3	9.1	9.9	10.3	12.1	14.7	10.6	11.9	14.7	10.5	13.4	18.7
$\mathcal{E}$ [10 <sup>51</sup> erg]	9.1	2.6	2.2	7.2	3.5	2.5	6.4	2.1	1.9	7.4	2.7	3.2
$\mathcal{N}$ [10 <sup>56</sup> ]	5.7	1.3	1.0	4.4	1.8	1.0	3.8	1.1	0.8	4.4	1.3	1.1
$\eta$	3.8	3.0	2.2	5.2	5.1	4.1	4.4	4.4	2.5	3.6	2.1	1.8

TABLE I: Keil parameters, mean energy  $\langle E_\alpha \rangle$ , energy emission  $\mathcal{E}_\alpha$ , total number emitted  $\mathcal{N}_\alpha$  ( $n_\alpha$  integrated over time), and pinching  $\eta_\alpha$ , of SN neutrino emissions for flavor  $\alpha$  as shown in Fig. 1.

where the oscillation probability  $P_{\alpha\beta} \equiv P(\nu_\beta \rightarrow \nu_\alpha)$  is given by

$$P_{\alpha\beta} = \sum_k |U_{\alpha k}|^2 |U_{\beta k}|^2. \quad (3)$$

Here  $U$  is the mass-flavor mixing matrix of neutrinos and the flavor  $\alpha$  runs for both neutrinos and antineutrinos. In terms of mixing angles,  $U$  is written as

$$U = \begin{pmatrix} 1 & 0 & 0 \\ 0 & \cos \theta_{23} & \sin \theta_{23} \\ 0 & -\sin \theta_{23} & \cos \theta_{23} \end{pmatrix} \begin{pmatrix} \cos \theta_{13} & 0 & \sin \theta_{13} e^{i\delta} \\ 0 & 1 & 0 \\ -\sin \theta_{13} e^{-i\delta} & 0 & \cos \theta_{13} \end{pmatrix} \begin{pmatrix} \cos \theta_{12} & \sin \theta_{12} & 0 \\ -\sin \theta_{12} & \cos \theta_{12} & 0 \\ 0 & 0 & 1 \end{pmatrix}, \quad (4)$$

where the values of the mixing angles are taken from [22]. This scenario is the same as astrophysical neutrinos traversing a long distance in vacuum before reaching the earth, and we thus denote it as vacuum oscillation (VO). Current measurements of mixing angles can be well-approximated by tri-bimaximal values so the fluxes can be described as [27]

$$F_e \cong \frac{5}{9} F_e^0 + \frac{4}{9} F_x^0, \quad (5)$$

$$F_{\bar{e}} \cong \frac{5}{9} F_{\bar{e}}^0 + \frac{4}{9} F_x^0, \quad (6)$$

$$4F_x \cong \frac{4}{9} F_e^0 + \frac{4}{9} F_{\bar{e}}^0 + \frac{28}{9} F_x^0, \quad (7)$$

where  $4F_x \equiv F_\mu + F_{\bar{\mu}} + F_\tau + F_{\bar{\tau}}$ .

In MSW scenarios, these fluxes shall be modified according to NMH when arriving at the

detector on Earth, and can be written as:

$$F_e = F_x^0, \quad (8)$$

$$F_{\bar{e}} = (1 - \bar{P}_{2e})F_{\bar{e}}^0 + \bar{P}_{2e}F_{\bar{x}}^0, \quad (9)$$

$$4F_x = F_e^0 + F_{\bar{e}}^0 + 4F_x^0 - F_e - F_{\bar{e}} = F_e^0 + \bar{P}_{2e}F_{\bar{e}}^0 + (3 - \bar{P}_{2e})F_x^0, \quad (10)$$

for the normal hierarchy, and

$$F_e = P_{2e}F_e^0 + (1 - P_{2e})F_x^0, \quad (11)$$

$$F_{\bar{e}} = F_{\bar{x}}^0, \quad (12)$$

$$4F_x = F_e^0 + F_{\bar{e}}^0 + 4F_x^0 - F_e - F_{\bar{e}} = (1 - P_{2e})F_e^0 + F_{\bar{e}}^0 + (2 + P_{2e})F_x^0, \quad (13)$$

for the inverted hierarchy [2]. Here  $P_{2e}$  ( $\bar{P}_{2e}$ ) is the probability that a mass eigenstate  $\nu_2$  ( $\bar{\nu}_2$ ) is observed as a  $\nu_e$  ( $\bar{\nu}_e$ ) since neutrinos arrive at the Earth as mass eigenstates. We do not consider the regeneration factor due to the Earth matter effect and thus take  $P_{2e} = \sin^2 \theta_{12}$ .

From these equations, it is shown that, in the normal hierarchy,  $\nu_e$  completely comes from  $\nu_x^0$  from the source while  $\bar{\nu}_e$  comes from both  $\bar{\nu}_e^0$  and  $\bar{\nu}_x^0$ . On the other hand, in the inverted hierarchy,  $\nu_e$  comes from both  $\nu_e^0$  and  $\nu_x^0$  while  $\bar{\nu}_e$  completely comes from  $\bar{\nu}_x^0$ .

### III. EVENT RATES OF SN NEUTRINOS IN TERRESTRIAL DETECTORS FOR THE NEUTRONIZATION BURST

With neutrino fluxes given above, we calculate event rates of SN neutrinos for all flavors,  $\nu_e$ ,  $\bar{\nu}_e$ , and  $\nu_x$ , for the vacuum oscillation (VO) scenario and the case that the flavor contents are modified by MSW effects as SN neutrinos propagate outward from the core. In the latter case, both normal and inverted hierarchies are taken into consideration and denoted as MSW-NH and MSW-IH scenarios, respectively. The event rates and quantities induced from these rates are displayed in numbers per bin with a 5 ms bin width throughout this article.

In liquid argon time projection chambers (LArTPC),  $\nu_e$  is the most easily detected species via its charged-current interaction with argon nuclei,  $\nu_e + {}^{40}\text{Ar} \rightarrow {}^{40}\text{K}^* + e^-$ . The cross section for this  $\nu_e\text{Ar}$  interaction has been computed in [23]. Numerical data compiled in [24] is used for our calculations. Assuming a SN at a distance of 5 kpc, the event rates of  $\nu_e\text{Ar}$  in DUNE are shown in Fig. 2. It is clearly seen that time-dependence profiles of the event rates for

the G-, B-, and F-models are similar while the pattern for the N-model is quite different. For the N-model, the event rate in VO scenario follows the  $\nu_e$  luminosity in shape with an obvious peak followed by a much lower tail in the later half of the period. On the other hand, in MSW scenarios, those rates increase to a maximum and then decrease very slowly or remain almost unchanged. With MSW effects, the rates in the inverted hierarchy are larger than those in the normal hierarchy in the beginning and becomes smaller in the latter times. The maxima in MSW scenarios can be larger than the peak in VO scenario because  $\nu_e$  and  $\nu_x$  fluxes swap differently in different scenarios and, in the N-models, the ratio of  $\nu_e$ Ar cross section at  $\langle E_{\nu_x} \rangle \sim 18.7$  MeV to that at  $\langle E_{\nu_e} \rangle \sim 10.5$  MeV is  $\gtrsim 7$ . Combining these facts and the flux information in Fig. 1, the ranking of event rates in different scenarios can be inferred by simple estimation.

For the G-, B-, and F-models in the peak region, the event rates in VO scenario are larger than those in MSW scenarios, in which the rates for NH are larger than those for IH. This ranking follows the ordering of Eqs. (5) > (11) > (8), where  $P_{2e} \cong 1/3$  and  $F_x^0$  is negligible compared to  $F_e^0$  in the peak region. In the long tail,  $F_e^0$  and  $F_x^0$  are both small and comparable to each other so, after fully or partially swap, event rates in different scenarios are indistinguishable with uncertainties taken into account. The event rate at the peak in VO scenario is about three half of that in MSW-IH scenario, and there is even no peak appearing in MSW-NH scenario. This is again due to the full or partial swap between  $\nu_e$  and  $\nu_x$  fluxes in MSW scenarios.

In VO scenario, the  $\nu_e$ Ar event rate at the peak in the N-model is about two-thirds of that in the G- and F-models while emission  $n_{\nu_e}$  at the peak in the N-model is about one half of that in the G- and F-models. This arises from the partial swap between  $\nu_e$  and  $\nu_x$  fluxes and larger  $\langle E_{\nu_x} \rangle$  in the N-model. In the B-model, the  $\nu_e$ Ar event rate exhibits no clear peak because the rate peaks near  $t = 0.5$  ms where is just the boundary between two adjacent bins. On the other hand, the  $\nu_e$ Ar event rates in the N-model are much larger than those in the other models in MSW scenarios at later times. To account for this, we note that both  $n_{\nu_x}$  and  $\langle E_{\nu_x} \rangle$  in the N-model are larger than those in the other models. Since  $\nu_e$ Ar cross section increases rapidly with the neutrino energy, the full or partial swapping between  $\nu_e$  and  $\nu_x$  fluxes in MSW scenarios hence favors the  $\nu_e$ Ar event rates in the N-model.

Table II presents total event numbers of the calculated event rates shown in Fig. 2. Given the fact that the total energy output and particle emission in all models follow the ordering

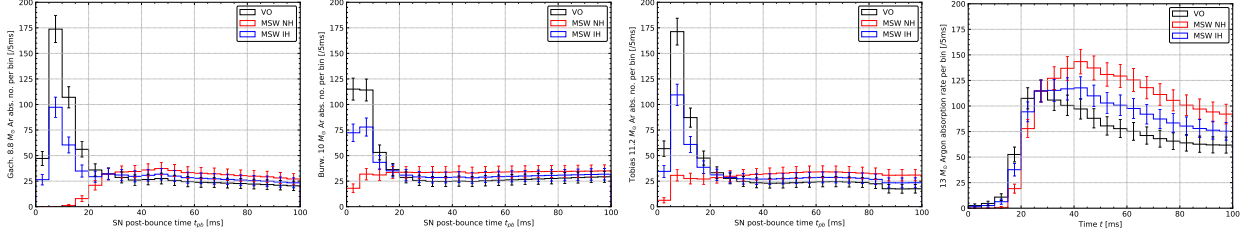


FIG. 2: Event rates of  $\nu_e$ Ar in DUNE in different flavor transition scenarios. These event rates are obtained in the G-, B-, F-, and N-models for progenitor masses of  $8.8 M_\odot$ ,  $10 M_\odot$ ,  $11.2 M_\odot$ , and  $13 M_\odot$  from left to right, respectively.

Simulation model [ $M_\odot$ ]	G	B	F	N
Vacuum Osc.	792	746	738	1373
MSW-NH	513	659	604	1861
MSW-IH	668	708	678	1590

TABLE II: Total numbers of SN neutrino events for  $\nu_e$ Ar signals in different flavor transition scenarios within the period of interest.

of  $N > B > F > G$ , total event numbers in different scenarios also follow this ordering. The total energy output and particle emission in the F-model are both about 80% of those in the B-model, rendering similar overall mean energies for the two models. Concerning  $\nu_e$ Ar detection mode, the total events in different scenarios follow the ordering of  $VO > MSW-IH > MSW-NH$ , reflecting the ordering of the  $\nu_e$  fluxes of Eqs. (5)>(11)>(8).

Besides these signals of interests, SN neutrinos also interact in the following channels in LAr TPC detectors:  $\nu + e^- \rightarrow \nu + e^-$  and  $\bar{\nu}_e$ Ar charged-current interaction,  $\bar{\nu}_e + {}^{40}\text{Ar} \rightarrow {}^{40}\text{Cl}^* + e^+$ . The event rates of the above channels are subdominant compared to  $\nu_e$ Ar interactions (for a reference, see Table II in [25] and Table I in [26]). Therefore, we neglect their contributions and focus on  $\nu_e$ Ar interactions.

#### IV. TESTING THE PRESENCE OF MSW EFFECTS

To account for the sharp rise of  $\nu_e$  flux during the neutronization burst, we define cumulative time distributions of the SN neutrino signals for the time interval of interest  $t = 0 - 0.1\text{s}$



as in [13]

$$K(t) = \frac{\int_0^t \frac{dN}{dt} dt}{\int_0^{0.1s} \frac{dN}{dt} dt}. \quad (14)$$

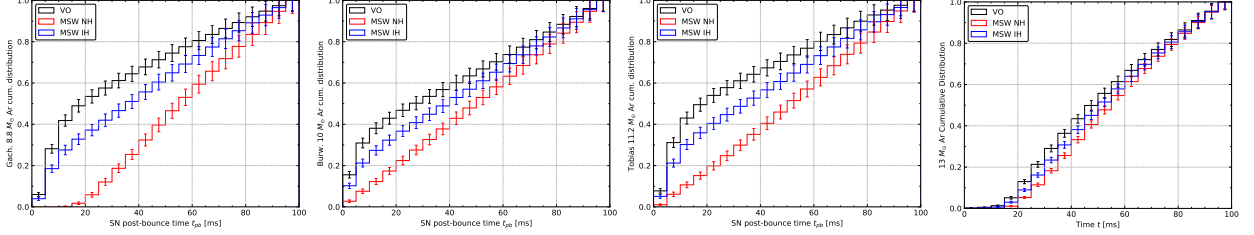


FIG. 3: Cumulative distribution of  $\nu_e \text{Ar}$  signals in the time period of  $0 \leq t \leq 0.1$  s. These event rates are obtained in the G-, B-, F-, and N-models for progenitor masses of  $8.8 M_\odot$ ,  $10 M_\odot$ ,  $11.2 M_\odot$ , and  $13 M_\odot$  from left to right, respectively.

In Fig. 3, we present  $K_{\text{Ar}}$  the cumulative distributions of  $\nu_e \text{Ar}$  event rates in VO, MSW-NH, and MSW-IH scenarios. By definition,  $0 \leq K(t) \leq 1$ . It is clearly seen that, on the upper panel, the cumulative  $\nu_e \text{Ar}$  signals in different scenario follow the relation,  $K_{\text{Ar}}^{\text{VO}} > K_{\text{Ar}}^{\text{IH}} > K_{\text{Ar}}^{\text{NH}}$ . In the G-, B-, and F-models, due to the significant differences of  $\nu_e \text{Ar}$  event rates between various scenarios in the peak region, the cumulative  $\nu_e \text{Ar}$  event rates for different scenarios can be clearly discriminated. In addition, because of the sharp peak,  $K(t)$  increases rapidly at initial times and then slowly grows to  $K(t) = 1$  in the end. In the N-model, the differences between the cumulative event rates in different scenarios are much smaller since the  $\nu_e \text{Ar}$  event rates exhibit no sharp peak in the initial times.

To clearly distinguish the vacuum oscillation from MSW oscillations, a ratio between the cumulative distributions is defined as

$$R_{\text{cum}}(t) \equiv \frac{2}{3} \left( \frac{1 + K_{\text{Ar}}(t)}{1 + N(t)} \right) - \frac{1}{3}. \quad (15)$$

Here  $N(t) = 10t$ , with  $t$  in seconds, represents the cumulative distribution of a constant event rates.  $R$  actually defines the distances from the diagonal,  $N(t)$ , to the cumulative event rates,  $K(t)$ . From  $K_{\text{Ar}}(0) = 0$ ,  $K_{\text{Ar}}(0.1 \text{ s}) = 1$ , one has  $R_{\text{cum}}(0) = R_{\text{cum}}(0.1 \text{ s}) = 1/3$ . The ordering,  $K_{\text{Ar}}^{\text{VO}} > K_{\text{Ar}}^{\text{IH}} > K_{\text{Ar}}^{\text{NH}}$  renders  $R_{\text{cum}}^{\text{VO}} > R_{\text{cum}}^{\text{IH}} > R_{\text{cum}}^{\text{NH}}$  as shown in Fig. 4.

Like the primary  $\nu_e$  emissions and  $\nu_e \text{Ar}$  event rates, the patterns of  $R_{\text{cum}}$  in the G-, B-, and F-models are completely different from that of the N-model. In the former three models,  $R_{\text{cum}}$  is a good discriminator to distinguish vacuum oscillation from MSW oscillations. In VO

scenario, the maxima of the  $R$  ratio in all the three models are larger than 0.5,  $R_{max}^{VO} \gtrsim 0.5$  and the maxima in MSW scenarios are smaller than 0.45,  $R_{max}^A \lesssim 0.45$ , with  $A$  being IH or NH. One can see that black curves for  $R_{cum}$  in vacuum oscillation scenario and colored curves for  $R_{cum}$  in MSW scenarios are clearly discriminated. Hence,  $R_{max}$  the maximum of  $R_{cum}$  determines whether or not MSW effects occur in the propagation of SN neutrinos.

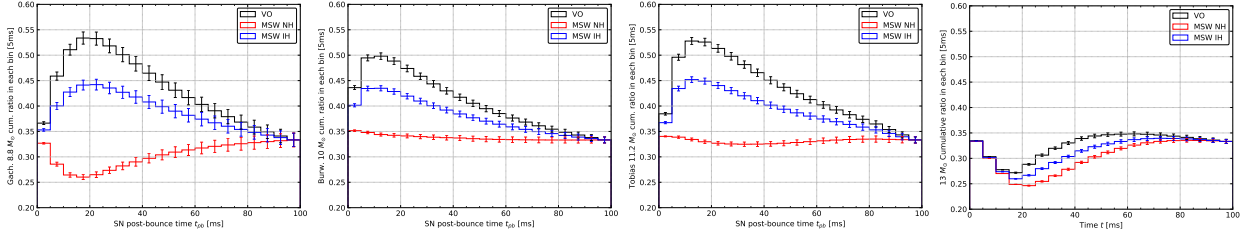


FIG. 4:  $R_{cum}$  in the time period of  $0 \leq t \leq 0.1$  s. These event rates are obtained in the G-, B-, F-, and N-models for progenitor masses of  $8.8 M_{\odot}$ ,  $10 M_{\odot}$ ,  $11.2 M_{\odot}$ , and  $13 M_{\odot}$  from left to right, respectively.

However, the discriminator  $R_{max}$  cannot be applied to the event rates in the N-model, in which  $R_{cum} \lesssim 0.35$  in all scenarios. From the definition of  $R_{cum}$ , Eq. (15), this indicates that  $K_{Ar}$  in the N-model is below the diagonal,  $N(t)$ , most of the time. Due to slowly-growing  $\nu_e Ar$  emission at initial times with a blunt peak of a lower height and broader width, the  $\nu_e Ar$  event rates in this case exhibit no clear peak. Consequently, the cumulative rates  $K_{Ar}$  and resultant ratio  $R_{cum}$  cannot be clearly distinguished between different flavor transition scenarios. Hence,  $R_{max}$  is not a good discriminator in the N-model.

We should note that, according to the current understanding of SN physics, in the early stage of the SN explosion, a sharp peak emerges in the profile of primary  $\nu_e$  emissions during the neutronization burst as shown in the G-, B-, and F-models in Fig. 1. Therefore, our method is effective in determine whether MSW effects occur or not although N-model does give rise to very distinctive  $R_{cum}$ .

## V. SUMMARY AND CONCLUSIONS

We have proposed to verify MSW effects in SN neutrinos by using the time evolution of SN neutrino event rates during the neutronization burst. These event rates are calculated with SN neutrino emissions extracted from SN simulation data of four groups, denoted as

the G-, B-, F-, and N-models [19, 20]. The behaviors of neutrino emissions in the four models are analyzed.

Given event rates of  $\nu_e\text{Ar}$  in liquid argon detectors, we define a cumulative event ratio  $R_{\text{cum}}$  in Eq. (15). We then demonstrate that time-evolution patterns of  $R_{\text{cum}}$  are effective in determining whether MSW effects occur in SN neutrino propagations or not. It is seen that the maximum of the cumulative ratio  $R_{\text{cum}}(t)$  is a good discriminator capable of confirming the MSW effects in SN neutrinos for G-, B-, and F-models. The basis of our method is the unique pattern of the primary  $\nu_e$  emission, which is different from the shapes of  $\bar{\nu}_e$  and  $\nu_x$  emissions. Vacuum and MSW oscillations moderate the sharp peak of  $\nu_e\text{Ar}$  event rates to different levels as seen in Fig. 2. The differences are manifested by the cumulative event rates  $K_{\text{Ar}}$ . Hence  $R_{\text{cum}}(t)$  constructed from  $\nu_e\text{Ar}$  events rates is a good test to MSW oscillations in SN neutrinos.

The ratio variables we use are derived from event rates of  $\nu_e\text{Ar}$  in terrestrial detectors and these event rates are calculated with SN neutrino emissions extracted from SN simulation data. We perform our analysis with simulation data of progenitor masses of 8.8, 10, 11.2, and 13  $M_\odot$  from four different simulation groups. Our work not only covers the mass range of the core-collapse SNe with iron-core but also takes different simulation approaches to SN neutrino emissions into account. Although our method does not work for the N-model, we note that the time evolutions of the neutrino emissions and their luminosity curves in the G-, B-, and F-models exhibit common behaviors, which agree with current understandings of neutrinos emissions of SN explosions. On the contrary, the predictions by the N-model deviates significantly from the current consensus. Based on the consensus of the SN neutrino emissions, our method is capable of determining whether MSW effects for neutrino propagations occur or not in all core-collapse SNe with iron-cores.

### Acknowledgements

The work is by the Ministry of Science and Technology, Taiwan under Grant No. 107-2119-M-009-017-MY3.

---

- [1] A. Mirizzi, I. Tamborra, H. T. Janka, N. Saviano, K. Scholberg, R. Bollig, L. Hudepohl and S. Chakraborty, Riv. Nuovo Cim. **39** (2016) no.1-2, 1, arXiv:1508.00785
- [2] A. S. Dighe and A. Y. Smirnov, Phys. Rev. D **62**, 033007 (2000), arXiv:hep-ph/9907423.
- [3] H. Duan, G. M. Fuller, J. Carlson and Y. Z. Qian, Phys. Rev. D **74** (2006) 105014, astro-ph/0606616.
- [4] S. Hannestad, G. G. Raffelt, G. Sigl and Y. Y. Y. Wong, Phys. Rev. D **74**, 105010 (2006), Phys. Rev. D **76**, 029901 (2007), astro-ph/0608695.
- [5] H. Duan, G. M. Fuller and Y. Z. Qian, Ann. Rev. Nucl. Part. Sci. **60**, 569 (2010), arXiv:1001.2799.
- [6] R. F. Sawyer, Phys. Rev. D **72** (2005) 045003, hep-ph/0503013.
- [7] R. F. Sawyer, Phys. Rev. D **79** (2009) 105003, arXiv:0803.4319.
- [8] R. F. Sawyer, Phys. Rev. Lett. **116** (2016) no.8, 081101, arXiv:1509.03323.
- [9] S. Chakraborty, R. S. Hansen, I. Izaguirre and G. Raffelt, JCAP **1603** (2016) 042, arXiv:1602.00698.
- [10] C. Lunardini and A. Yu Smirnov, J. Cosm. Astropart. Phys. **06**, 009 (2003), arXiv:hep-ph/0302033.
- [11] B. Dasgupta, A. Dighe, A. Mirizzi, Phys. Rev. Lett. **101** 171801 (2008), arXiv:08021481.
- [12] H. Duan, G. M. Fuller, J. Carlson, Y. Z. Qian, Phys. Rev. Lett. **99**, 241802 (2007), arXiv:0707.0290.
- [13] P. D. Serpico, S. Chakraborty, T. Fischer, L. Hudepohl, H. T. Janka and A. Mirizzi, Phys. Rev. D **85** (2012) 085031, arXiv:1111.4483.
- [14] S. H. Chiu, C.-C. Huang, and K.-C. Lai, PTEP 2015 6, 063B01(2015), arXiv:1312.4262.
- [15] K.-C. Lai, F.-F. Lee, F.-S. Lee, G.-L. Lin, T.-C. Liu and Y. Yang, JCAP **1607**, no. 07, 039 (2016), arXiv:1603.00692.
- [16] D. Vale, T. Rauscher and N. Paar, JCAP **1602** (2016) 007, arXiv:1509.07342.

- [17] L. Hudepohl, B. Muller, H.-T. Janka, A. Marek and G. G. Raffelt, Phys. Rev. Lett. **104** (2010) 251101, Erratum: Phys. Rev. Lett. **105** (2010) 249901, arXiv:0912.0260.
- [18] A. Burrows, D. Radice and D. Vartanyan, Mon. Not. Roy. Astron. Soc. **485** (2019) no.3, 3153, arXiv:1902.00547.
- [19] T. Fischer, G. Martinez-Pinedo, M. Hempel, L. Huther, G. Ropke, S. Typel and A. Lohs, EPJ Web Conf. **109** (2016) 06002, arXiv:1512.00193.
- [20] K. Nakazato, K. Sumiyoshi, H. Suzuki, T. Totani, H. Umeda and S. Yamada, Astrophys. J. Suppl. **205** (2013) 2, arXiv:1210.6841.
- [21] M. T. Keil, G. G. Raffelt, and H.-T. Janka, Astrophys. J. **590**, 971 (2003), arXiv:astro-ph/0208035.
- [22] P. A. Zyla et al. (Particle Data Group), to be published in Prog. Theor. Exp. Phys. 083C01 (2020).
- [23] E. Kolbe, K. Langanke, G. Martinez-Pinedo and P. Vogel, J. Phys. G **29** (2003) 2569, nucl-th/0311022.
- [24] K. Scholberg, Ann. Rev. Nucl. Part. Sci. **62** (2012) 81, arXiv:1205.6003.
- [25] C. Lujan-Peschard, G. Pagliaroli and F. Vissani, JCAP **1407**, 051 (2014), arXiv:1402.6953.
- [26] Jia-Shu Lu, Yu-Feng Li and Shun Zhou, Phys. Rev. D **94**, 023006 (2016), arXiv:1605.07803.
- [27] In our calculations, best-fit values of mixing angles are adapted.